ADVANCED FUNCTIONAL MATERIALS
www.afm-journal.de

Toward High Energy Organic Cathodes for Li-Ion Batteries: A Case Study of Vat Dye/Graphene Composites

Wei Ai, Weiwei Zhou, Zhuzhu Du, Chencheng Sun, Jun Yang, Yu Chen, Zhipeng Sun, Shun Feng, Jianfeng Zhao, Xiaochen Dong, Wei Huang, and Ting Yu**

Despite the fascinating Li storage properties of organic carbonyl compounds, e.g., high therotical capacity and fast kinetics, it is still lack of a facile and effective way that capable of large-scale producion of advanced carbonyl cathodes for Li-ion batteries (LIBs). Here, a generic strategy is proposed by combining sonication and hydrothermal techniques for scalable synthesis of high performance organic carbonyl cathodes for LIBs. A series of commercialized vat dyes with abundant electroactive conjugated carbonyl groups are confined in between the graphene layers, forming a compatible 3D hybrid architecture. The unique structure affords good Li^+ ions accessibility to the electrode and short Li^+ ions diffusion length. Meanwhile, each sandwiched graphene layer functions as a miniature current collector, ensuring fast electron transport throughout the entire electrode. Consequently, the cathodic performances of LIBs using the composites as electrodes, for example, Vat Green 8/graphene, Vat Brown BR/graphene, and Vat Olive T/graphene, possess high specific capacity, exceptional cycling stability, and excellent rate capability. The effect of vat dye content on the morphology, structure, and the final electrochemical performance of the composites is investigated as well. This work provides a versatile and low-cost platform for large-scale development of advanced organic-based electrodes toward sustainable energy fields.

1. Introduction

Concerns about environmental degradation and energy crisis promote the exploitation of green and sustainable natural resources, e.g., solar and wind powers. Since these energy sources are typically intermittent and localized, they must be efficiently stored prior to proper use and transportation.[1] As such, energy storage naturally becomes one of the most important topics in the 21st century, and has received worldwide concerns in the past few years.[2] Among various energy storage devices, Li-ion battery (LIB) is the most promising candidate featured by its superior energy storage capability in terms of output energy typically exceeding 90% of input energy, except at the highest power density.[3] Since the birth in 1990s, LIB has been the dominant power source for portable electronics. Nevertheless, the development of LIB cannot keep pace with the ever-growing demand for energy, especially the emergent electric vehicles and smart grids. Further increasing the energy storage capability of LIB requires the boost of specific capacities of the electrode materials. In particular, the cathode side, since the practical capacities of traditional inorganic insertion-type cathodes are normally limited to 200 mAh g^{-1} associated with one electron reaction, thus bringing about a bottleneck for further breakthroughs in LIB performance.[4,5] Forturnately, organic cathodes are

W. Ai, Z. Du, C. Sun, J. Yang, Prof. J. Zhao, Prof. X. Dong, Prof. W. Huang
Key Laboratory of Flexible Electronics (KLOFE) & Institute of Advanced Materials (IAM)
National Jiangsu Synergistic Innovation Center for Advanced Materials (SICAM)
Nanjing Tech University (NanjingTech)
30 South Puzhu Road, Nanjing 211816, China
E-mail: iamwhuang@njtech.edu.cn

W. Ai, Y. Chen, S. Feng, Prof. T. Yu
Division of Physics and Applied Physics
School of Physical and Mathematical Sciences
Nanyang Technological University
637371, Singapore
E-mail: yuting@ntu.edu.sg

Prof. W. Zhou
School of Materials Science and Engineering
Harbin Institute of Technology at Weihai
Weihai 264209, China

Prof. Z. Sun
Key Laboratory of Materials and Technology for Clean Energy
Ministry of Education
Key Laboratory of Advanced Functional Materials
Xinjiang University
Urumqi 830011, China

Prof. W. Huang
Key Laboratory for Organic Electronics & Information Displays (KLOEID) and Institute of Advanced Materials (IAM)
Nanjing University of Posts & Telecommunications
Nanjing 210023, Jiangsu, China

Prof. T. Yu
Department of Physics
Faculty of Science
National University of Singapore
117542, Singapore

DOI: 10.1002/adfm.201603603

capable of providing multielectron reactions compared with their inorganic counterparts, and hence higher theoretical capacity.[6] Moreover, organic cathodes have several distinctive advantages of low molecular weight, structural diversity, and redox potential adjustment.[7–9] More strikingly, organic cathodes could be directly extracted from abundant/renewable biomass precursors and then recycled through photosynthesis, thus making the concept of "green and sustainable" LIBs possible.[10,11]

In the pursuit of high performance organic electrodes, organic carbonyl compounds containing single or multiple conjugated electrochemically active carbonyls have been overwhelmingly studied owing to their high capacity and intrinsically fast kinetics.[12,13] Each carbonyl can undergo a reversible one electron transfer reaction during charge and discharge processes, that is, one electron reduction to generate monoanion and thereafter one electron oxidation to convert back to carbonyl. Indeed, the exploration of carbonyl cathodes could be traced back to the early 1969,[14] however, in most cases, these cathodes suffer from fast capacity decay due to their severe solubility in the electrolyte and poor rate capability arising from the low electronic conductivity. Aiming to tackle these issues, to date, diverse strategies including optimization of molecular structure,[15–17] immobilization of carbonyl species on conducting matrix/substrates,[18–20] polymerization of small molecule carbonyls,[21–23] and employment of solid-state electrolytes[24–26] have been proposed. Recently, it has been demonstrated that constructing carbon-supported organic composites is another effective and intriguing approach for achieving advanced organic cathodes.[27] As a result, a series of carbonyl/carbon composites with significantly improved electrochemical performances have been prepared by means of solution mixing,[28] ball milling,[29] impregnation,[30] in situ polymerization,[31] self-assembly,[32] and chemical vapor deposition[33] methods. Despite these achievements, till now, it still remains a great challenge to prepare carbonyl/carbon composites with high and uniform quality on a large scale before their practical applications become possible. Note that the commercially available carbonyl products, for example, vat dyes, are desirable cathodes capable of mass production because they can now be readily obtained from plants or synthesized artificially.[34] Nevertheless, to the best of our knowledge, vat dyes which are normally used for fabric dyeing has not been reported as the cathode for LIBs.

Herein, for the first time we develop a universal method, that is, a combination of sonication and hydrothermal process, to scalable synthesis of vat dye/graphene composites as novel organic cathodes for high performance LIBs. As a representative example of vat dyes, Vat Green 8 (molecular structure shown in **Figure 1**) is a green color dye containing a large condensed aromatic ring system with electroactive conjugated carbonyl groups, making it perfect electrode for LIBs. We propose that the π–π interactions between Vat Green 8 and graphene sheets afford a stable composite structure, which can not only effectively suppress the dissolution of active material but also guarantee fast electron transportation during the electrochemical reactions. In this case, the aforementioned two common issues of organic electrodes could be simultaneously and effectively solved in our system. Consequently, the Vat Green 8/graphene (VG 8/G) composite exhibits long-term cyclic stability and excellent high-rate capability. This simple and elegant design can also readily extended to fabricate Vat Brown BR/graphene (VB BR/G) and Vat Olive T/graphene (VO T/G) composites, showing exceptional electrochemical performance, which verifies the universality of our method. Importantly, the present strategy provides a scalable route for developing advanced organic cathodes for LIBs, making a significant step forward to their practical applications.

2. Results and Discussion

Figure 1 depicts the scheme for the synthesis of VG 8/G composite. Briefly, Vat Green 8 was first dispersed into graphene oxide (GO) aqueous solution with different weight ratios under continuous sonication, which was then subjected to hydrothermal reaction and freeze-drying sequentially (see the Experimental Section for details). The formation of VG 8/G hybrid architecture experiences the initial disassembly of Vat Green 8 crystal structure and the following reassembly on the graphene sheets through the π–π interactions between them.[35,36] The resultant product was denoted as VG 8/G-X, where X represents the weight ratio of Vat Green 8 to GO. **Figure 2**a,b presents the schematic structures of Vat Green 8 and VG 8/G composites for Li storage. Due to strong intermolecular interactions, Vat Green 8 alone tends to self-assemble into a stacking structure, resulting in greatly diminished accessible active sites and long diffusion length for Li^+ ions. In contrast, when

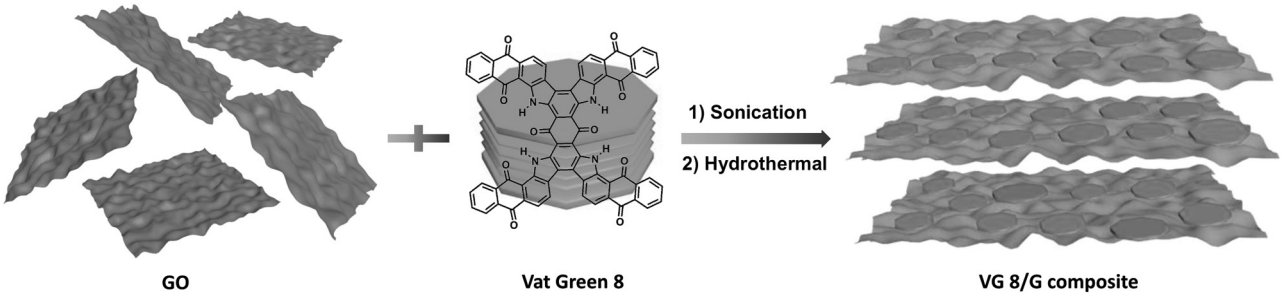

Figure 1. Schematic illustration of the synthesis of VG 8/G composite, which was formed through the disassembly of Vat Green 8 crystal structure and then reassembly on the graphene sheets. The main driving force for the formation of VG 8/G hybrid architecture is the π–π interactions between Vat Green 8 and graphene sheets.

Adv. Funct. Mater. **2016**,
DOI: 10.1002/adfm.201603603

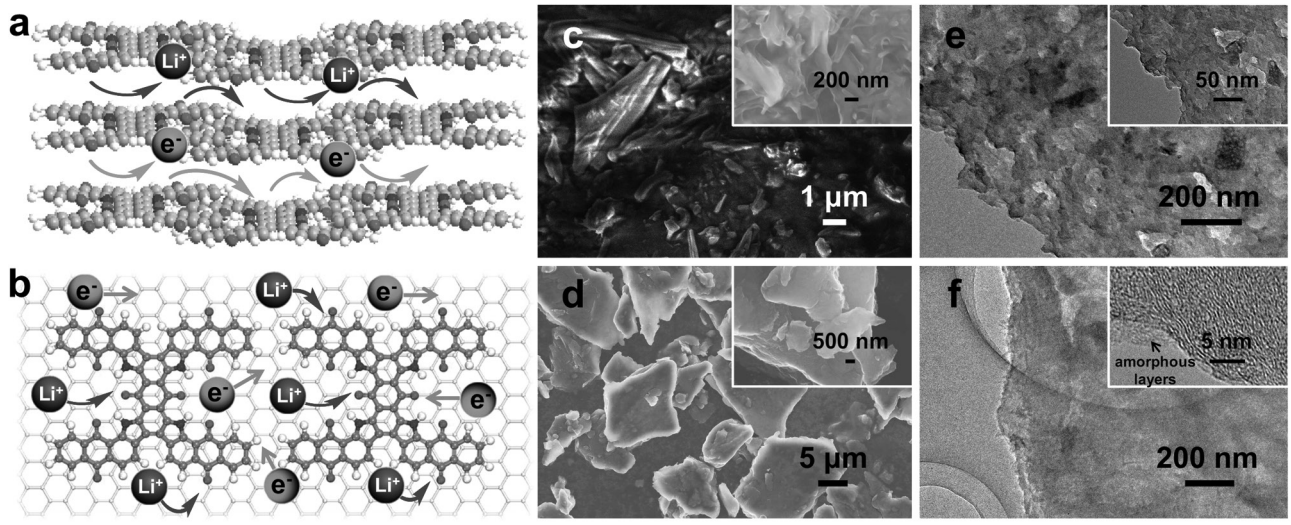

Figure 2. Schematic structures of a) Vat Green 8 and b) VG 8/G composites for Li storage. FESEM images of c) Vat Green 8 and d) VG 8/G-0.5. The insets are higher-magnification FESEM image of the corresponding samples. e) TEM image of Vat Green 8. Inset: higher-magnification TEM image. f) TEM image of VG 8/G-0.5. Inset: HRTEM image of VG 8/G-0.5.

integrated with graphene, the aromatic Vat Green 8 molecules can absorb tightly on the surface of graphene sheets through π–π interactions, hence more desirable for Li storage in terms of better Li^+ ions accessibility, shorter Li^+ ions diffusion paths and higher electronic conductivity. Field-emission scanning electron microscopy (FESEM) images show that pristine Vat Green 8 is composed of microsized bulk particles due to the spontaneous stacking of molecules (Figure 2c), whereas bare reduced graphene oxide (rGO) exhibits an interconnected 3D porous network with randomly distributed pores that are consisted by graphene thin layers (Figure S1a,b, Supporting Information). Interestingly, the VG 8/G composites display an appealing 3D graphite-like structure with Vat Green 8 molecules confined in between the graphene layers (Figure 2d and Figure S1c–f, Supporting Information). Note that excess Vat Green 8 would generate bulk particles in the composite, as observed in the FESEM image of VG 8/G-1 (Figure S1e,f, Supporting Information). The microstructure of the samples was further studied by transmission electron microscopy (TEM). The Vat Green 8 molecules show an asphaltum-like morphology with densely stacked structure (Figure 2e), while rGO presents a smooth and transparent thin layer with wrinkled and folded edges (Figure S1g, Supporting Information). However, after the incorporation of Vat Green 8 on the graphene sheets, VG 8/G-0.5 exhibits thick layers and rough surfaces (Figure 2f). Moreover, no evident bulk Vat Green 8 is viewed, indicating the Vat Green 8 is well embedded in between the graphene layers. This is further confirmed by high-resolution TEM (HRTEM) images. As shown in the inset of Figure 2f, VG 8/G-0.5 reveals the presence of amorphous layers representing the absorbed Vat Green 8 molecules, which are not detected in bare rGO (Figure S1h, Supporting Information).

X-ray photoelectron spectroscopy (XPS) technique was applied to examine the elemental composition of the samples. **Figure 3**a shows the comparison of XPS survey spectra for GO and VG 8/G composites. The appearance of N 1s signal located at approximately 400 eV in VG 8/G composites yet not observed in GO suggests the existence of Vat Green 8 in the hybrids. Table S1 of the Supporting Information summarizes the elemental composition of the samples obtained from XPS measurements. The content of nitrogen increases from 1.29 at% in VG 8/G-0.25 to 1.38 at% in VG 8/G-0.5 and 2.14 at% in VG 8/G-1, indicating the increased amount of Vat Green 8 in the composite. Compared with GO, the VG 8/G composites exhibit substantially increased carbon content associated with considerably decreased oxygen content, which implies the efficient reduction of GO after the hydrothermal treatment. This is further evidenced by high-resolution C 1s XPS spectra shown in Figure 3b. The deconvolution of GO displays four peaks correspond to C—C (sp^2 carbon, 284.6 eV), C—O (hydroxyl/epoxy groups, 286.7 eV), C=O (carbonyl groups, 288.1 eV), and O—C=O (carboxyl groups, 289.2 eV). In the spectra of VG 8/G composites, the oxygen functional species show significantly decreased intensity compared to that of GO, demonstrating the removal of oxygen-containing groups with concomitant reconstruction of sp^2 carbon network. Besides, an additional peak located at 285.6 eV is detected, which originates from the C—N bonds of Vat Green 8 molecules. High-resolution N 1s XPS spectra of the VG 8/G composites (Figure 3c) exhibit a single predominant peak at about 399.9 eV, assignable to the pyrrole-like N atoms, which agrees well with the N bonding configuration in Vat Green 8. These results document that the chemical structure of Vat Green 8 is well-preserved in the VG 8/G composites. Fourier transform infrared spectroscopy (FTIR) was also employed to analyze the structural information of the samples. As shown in Figure S2 of the Supporting Information, VG 8/G composites exhibit almost the same spectral features, e.g., peak position and peak intensity, as those of prinstine Vat Green 8 molecules. Therefore, it can be concluded that the achievement of VG 8/G hybrid architecture is merely a physical process without any structural variations of Vat Green 8 molecules.

Further structural analyses of the samples are obtained by X-ray diffraction (XRD), Raman spectroscopy and

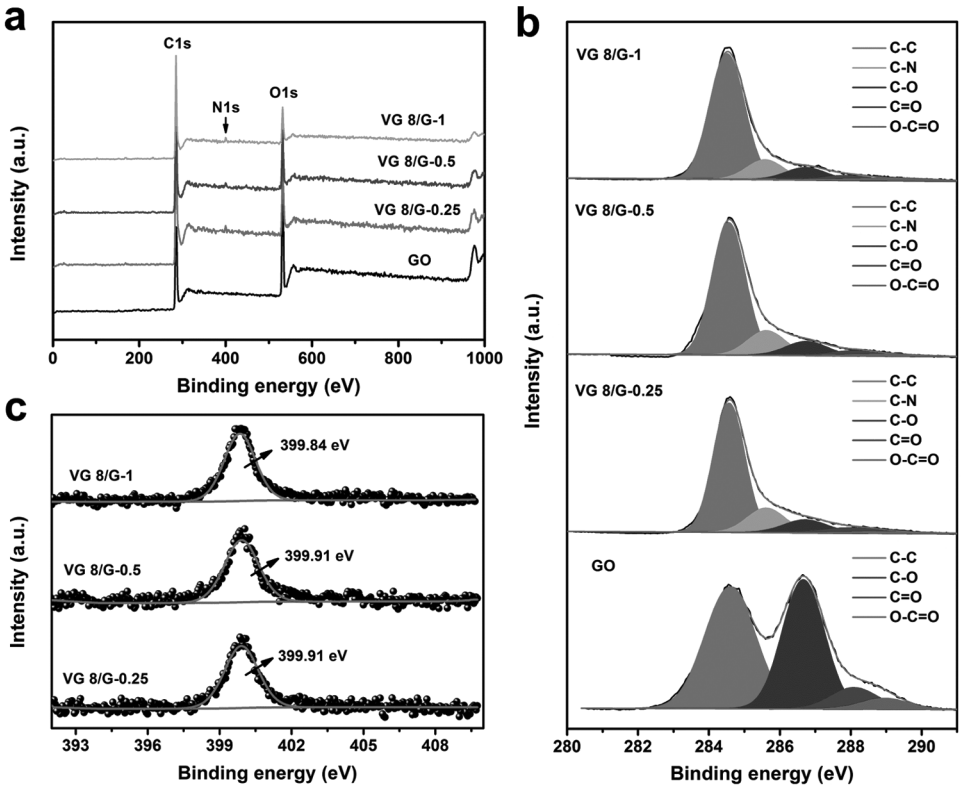

Figure 3. a) XPS survey spectra and b) high-resolution C 1s XPS spectra of GO, VG 8/G-0.25, VG 8/G-0.5, and VG 8/G-1. c) High-resolution N 1s XPS spectra of VG 8/G-0.25, VG 8/G-0.5, and VG 8/G-1.

thermogravimetric analysis (TGA) characterizations. **Figure 4**a depicts the XRD patterns of Vat Green 8 before and after hybridization. The bulk Vat Green 8 particles display three characteristic diffraction peaks located at 11.2°, 18.9°, and 26.1°, referring to the crystalline Vat Green 8 molecules. Interestingly, these peaks are not detected in the XRD patterns of VG 8/G-0.25 and VG 8/G-0.5, evidencing the disassembly of Vat Green 8 crystal associated with its reassembly on graphene sheets through π–π supramolecular interactions. However, excess Vat Green 8 precursor will induce the formation of bulk particles in the final composite. As a consequence, a diffraction peak at 11.2° which belongs to crystalline Vat Green 8 is observed in the XRD pattern of VG 8/G-1, corroborating previous FESEM results (Figure S1e,f, Supporting Information). Besides, all the three VG 8/G composites show a predominant diffraction peak at about 25.5°, which should be ascribed to the (002) plane of rGO. Compared with the sharp (002) peak of graphite at 26.5° (d spacing = 3.35 Å), the VG 8/G composites display a relatively broad peak with a slightly larger d spacing of 3.49 Å, which suggests their poorly ordered stacking due to the presence of Vat Green 8 molecules in between the graphene layers. Raman spectroscopy was used to probe the interaction between Vat Green 8 and graphene. As presented in Figure 4b, bare rGO exhibits two typical peaks at 1340 and 1586 cm^{-1}, corresponding to the breathing mode of A_{1g} symmetry (D band) and E_{2g} vibration mode of sp^2 C atoms (G band), respectively. Meanwhile, VG 8/G composites show quite similar spectral feature as compared to rGO except for the G band down-shifted to 1576 cm^{-1}. Such a clear shift of G band to lower frequency highly supports the charge transfer from the aromatic Vat Green 8 molecules to graphene sheets,[37,38] indicating the strong π–π interactions between them. TGA curves reveal that both Vat Green 8 and VG 8/G composites have good thermal stability up to over 300 °C (Figure 4c). All of the samples illustrate an initial weight loss of about 4.5% at temperature below 150 °C, attributable to the removal of physically adsorbed water. The samples are relatively stable at temperatures ranging from 150 to 300 °C. After that, a continuous and steady weight loss is observed with temperature inceases from 300 to 800 °C due to the carbonization of the Vat Green 8. To determine the content of Vat Green 8 in the composites, the samples are further characterizaed by elemental analysis (**Table 1**). The measured N contents in Vat Green 8, VG 8/G-0.25, VG 8/G-0.5, and VG 8/G-1 are 3.35, 1.03, 1.57, and 2.02 wt%, respectively. Therefore, the contents of Vat Green 8 are calculated to be 31.6 wt% in VG 8/G-0.25, 46.6 wt% in VG 8/G-0.5 and 60.3 wt% in VG 8/G-1.

The electrochemical performances of VG 8/G composites as cathodes for LIBs were evaluated using traditional 2032 coin-type cells with pure Li metal foils as the anodes. For comparison, the commercial Vat Green 8 is also tested uner the same conditions. **Figure 5**a shows the electrochemical Li storage mechanism of a single VG 8/G unit, which involves multi-step reduction of the conjugated carbonyl groups in Vat Green 8 molecule during discharge process and then reoxidation of the as-formed alkoxide groups in the subsequent charge process.[7,27] The presence of graphene can efficiently facilitate

DOI: 10.1002/adfm.201603603

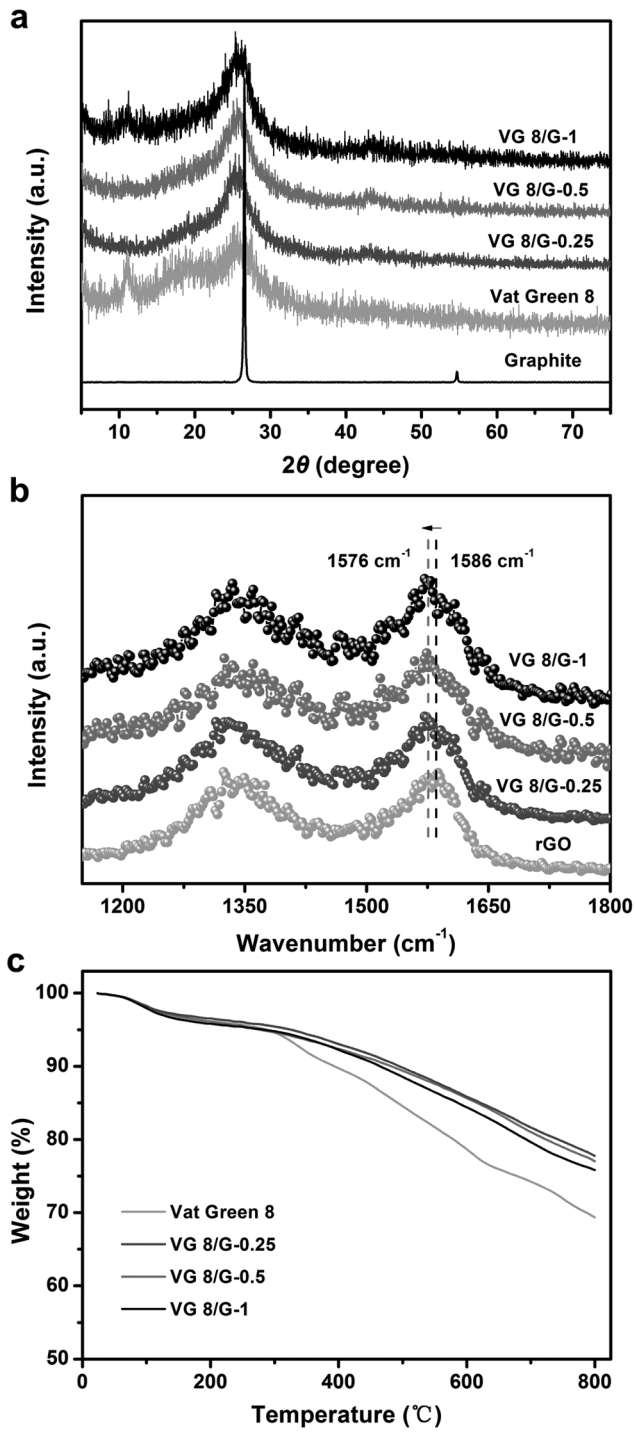

Figure 4. a) XRD patterns of Vat Green 8, graphite and VG 8/G composites. b) Raman spectra of rGO and VG 8/G composites using a 532 nm excitation laser. c) TGA curves of Vat Green 8 and VG 8/G composites under N_2 atmosphere.

charge transfer, leading to increased kinetics of electrochemical reactions. Cyclic voltammogram (CV) curves of different electrodes tested at 0.5 mV s^{-1} in the voltage range between 1.2 and 4.2 V (vs Li/Li^+) are presented in Figure 5b. Evidently, all the VG 8/G composites exhibits significantly improved gravimetric

Table 1. Elemental content of Vat Green 8 and VG 8/G composites obtained from elemental analysis. Each sample was tested twice, and the standard deviation for N content was determined to be <0.14 wt%.

Sample	N [wt%]	C [wt%]	H [wt%]
Vat Green 8	3.35	62.03	4.01
VG 8/G-0.25	1.03	75.37	1.81
VG 8/G-0.5	1.57	74.69	1.98
VG 8/G-1	2.02	72.49	2.61

current compared to that of Vat Green 8. The low current density should be attributed to its low electronic conductivity and the densely stacked structure, which induce limited accessibility to the electrolyte. After the disassembly and reassembly hybridization processes, these problems have been well addressed in the VG 8/G composites. With increasing the content of Vat Green 8 from ≈32 wt% (VG 8/G-0.25) to ≈47 wt% (VG 8/G-0.5) in the composite, the current density of VG 8/G composites exhibits an obvious increase trend. However, a dramastical decay of current density is observed when the value reaches ≈60 wt% (VG 8/G-1), due to the formation of bulk Vat Green 8 particles in the composite, as demonstrated by previous FESEM images (Figure S1e,f, Supporting Information). A pair of redox peaks at around 2.14 and 2.46 V correspond to the reduction of the conjugated carbonyl groups and reoxidation of the alkoxide groups, respectively. This matches well with the scheme shown in Figure 5a. The relative broad peaks are probably caused by the multistep reaction processes,[24,25] which can also be identified by the charge–discharge voltage profiles without obvious plateaus (Figure 5c).

Galvanostatic cycling tests of the electrodes are measured at 100 mA g^{-1} for 200 cylces (Figure 5d). It is predictable that the Vat Green 8 would exhibit poor Li storage behavior in terms of low capacity and fast capacity fading. The discharge capacity is as low as 9 mAh g^{-1} in the first cycle and decreased to 2 mAh g^{-1} after 200 cycles. On the contrary, the Li storage capacity and cyclic stability of VG 8/G composites have been extremely improved after immobilization of Vat Green 8 on the graphene sheets. The initial discharge capacities for VG 8/G-0.25, VG 8/G-0.5, and VG 8/G-1 are up to ≈240, ≈272, and ≈121 mAh g^{-1}, respectively, which maintain at ≈223, ≈319, and ≈153 mAh g^{-1} after 200 cycles. These values are definitely superior to previously reported organic cathodes,[39,40] functionalized carbon-based cathodes[18,41] and even some organic/carbon hybrid composite cathodes.[28,31] The slightly increase of capacity upon cycling observed in VG 8/G-0.5 and VG 8/G-1 might be ascribed to the delayed electrolyte infiltration into the electrodes.[42,43] With continuous charge-discharge processes, Li^+ ions could gradually go into the inner deep regions of the electrodes, leading to more available active sites for Li storage and hence a progressively raised capacity. To further examine their rate capability, the electrodes are tested under programmed current densities from 50 to 3200 mA g^{-1} (Figure 5e). It can be seen that the capacities of VG 8/G composites are consistently higher than those of Vat Green 8 throughout the whole rate cycles. In particular, the VG 8/G-0.5 electrode still shows the best rate performance with respect to other

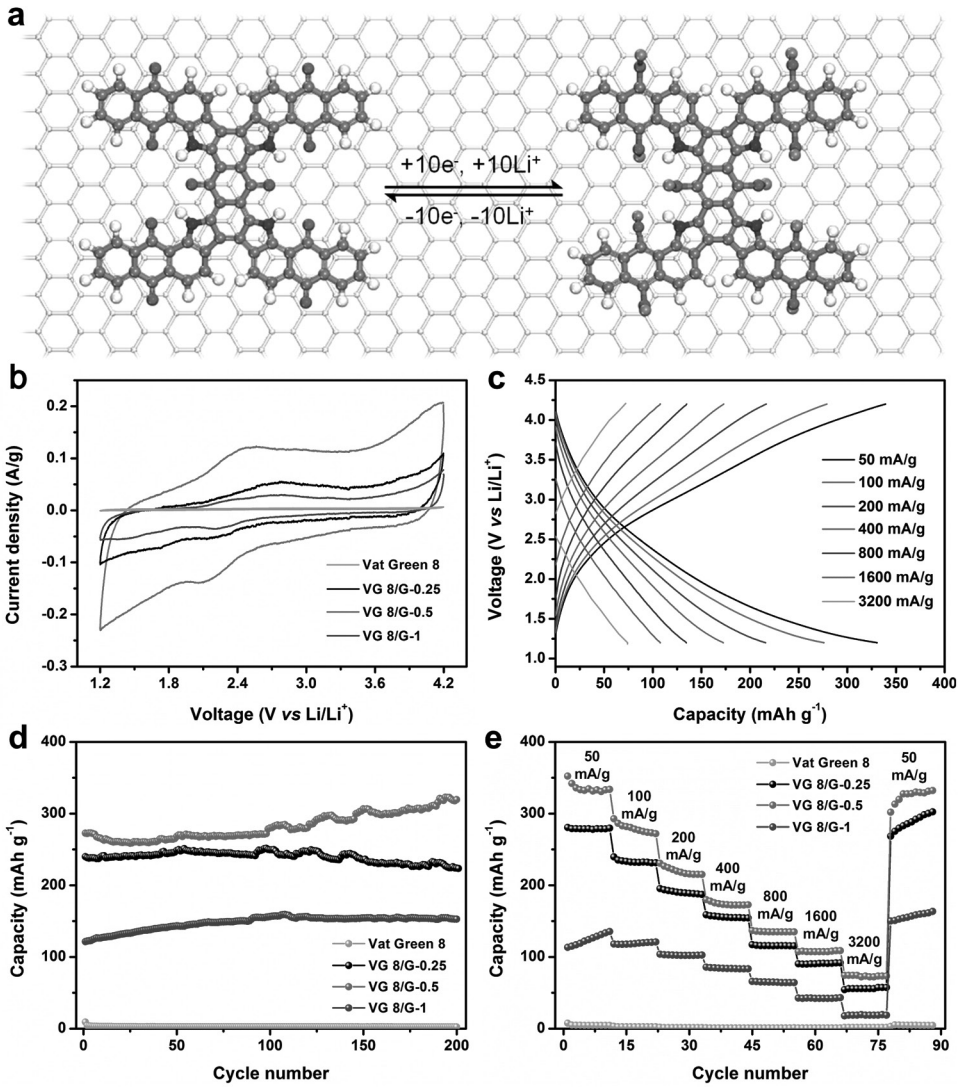

Figure 5. a) Electrochemical Li storage mechanism of a single VG 8/G unit. b) CV curves of different electrodes tested at 0.5 mV s^{-1}. c) Charge–discharge voltage profiles of VG 8/G-0.5 electrode under various current rates. d) Cycling performance of different electrodes measured at 100 mA g^{-1}. e) Rate performance of different electrodes under various current rates.

electrodes (VG 8/G-0.25, VG 8/G-1), which should be related to its moderate loading content of the electrochemically active Vat Green 8 associated with the as-formed peculiar nanostructure (see previous discussions). The capacities of VG 8/G-0.5 electrode obtained at 50, 100, 200, 400, 800, 1600, and 3200 mA g^{-1} are ≈330, ≈274, ≈216, ≈172, ≈135, ≈107, and ≈74 mAh g^{-1}, respectively. More strikingly, the capacity of VG 8/G-0.5 electrode is capable of gradual recovery to ≈332 mAh g^{-1} with the current density switched back to 50 mA g^{-1} after being tested at varied current densities, indicating its excellent rate capability.

To evaluate the kinetics of electrochemical reactions on the electrode, electrochemical impedance spectroscopy (EIS) was carried out in the frequency range of 100 kHz to 0.1 Hz (**Figure 6**). As shown in Figure 6a, the Nyquist plots of all the samples possess the same features with two semicircles in the high-to-medium frequency range and a tail (short inclined line) in the low frequency range, which can be successively assigned to the surface film impedances (R_{sf}) due to the solid electrolyte interphase (SEI) formation, charge transfer resistance (R_{ct}), and Warburg impedance.[44] The simulated values of EIS by using the equivalent circuit model (Figure 6b) are summarized in Figure 6c for better comparison. It can be seen that all the electrodes show comparable bulk resistance (R_b) that is related to the electrolyte and contact resistances. Nonetheless, the electrode of VG 8/G composites show substantially lower R_{sf} and R_{ct} compared to Vat Green 8, as reflected by the smaller semicircle at both high and middle frequency ranges in the Nyquist plots, demonstrating the enhanced kinetics of Li^+ ions migration through the SEI film and faster charge transfer reaction. Meanwhile, the short inclined lines with larger phase angles at low frequency region suggest lower Warburg impedance in VG 8/G composites, which represents the diffusion of Li^+ ions within the electrodes. As discussed in Figure 2a,b, in the crystalline Vat Green 8 electrode, Li^+ ions need to diffuse only along the intermolecular space to the entire electrode due to its stacked structure with limited exposure to the electrolyte.

DOI: 10.1002/adfm.201603603

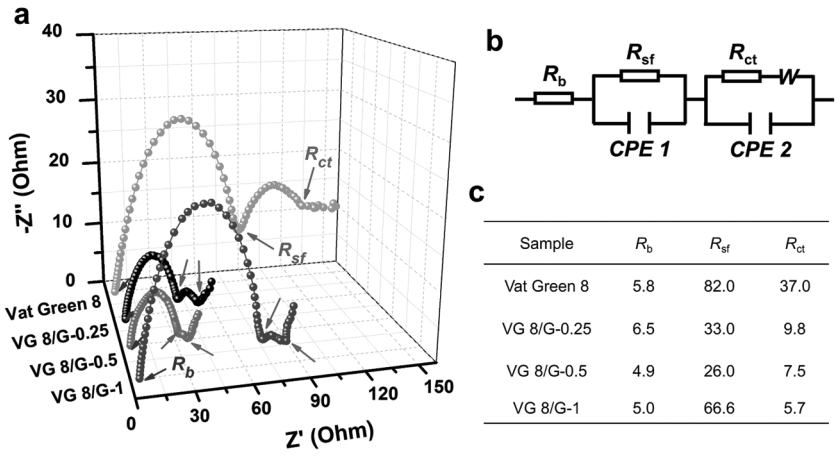

c

Sample	R_b	R_{sf}	R_{ct}
Vat Green 8	5.8	82.0	37.0
VG 8/G-0.25	6.5	33.0	9.8
VG 8/G-0.5	4.9	26.0	7.5
VG 8/G-1	5.0	66.6	5.7

Figure 6. a) Nyquist plots of the Vat Green 8, VG 8/G-0.25, VG 8/G-0.5, and VG 8/G-1 electrodes. The brown, green and pink arrows refer to the R_b, R_{sf}, and R_{ct}, respectively. b) The equivalent circuit model used for fitting the EIS. c) The fitting results for different electrodes.

In sharp contrast, the disassembled Vat Green 8 molecules are anchored on graphene layers, thus more readily accessible to Li^+ ions with shorter Li^+ ion diffusion paths. The above results exclusively identify the significantly improved electrochemical properties of VG 8/G composites over Vat Green 8 cathode. Such exceptional performances in terms of high capacity, long cyclic life, and outstanding rate capability mainly arise from the synergistic effects between Vat Green 8 molecules and graphene: first, the Vat Green 8 with substantial conjugated carbonyl groups primarily contributes to the Li storage capacity, whereas graphene with high electrical conductivity benefits the electron transfer. Second, the strong π–π interactions between Vat Green 8 and graphene sheets can effectively suppress the dissolution of Vat Green 8 into the electrolyte, thus guaranteeing high capacity retention. Third, the immobilization of disassembled Vat Green 8 molecules on graphene sheets facilitates easy accessibility of Li^+ ions to the electrode and accordingly ensures more active sites for Li storage with shorter Li^+ ion diffusion paths. Finally, the remaining oxygen functional groups on graphene can also contribute to the high Li storage capacity through surface redox reactions with Li^+ ions.

Besides VG 8/G, our method has also been successfully applied to fabricate other vat dye/graphene composites, such as Vat Brown BR/graphene (VB BR/G) and Vat Olive T/graphene (VO T/G) (Molecular structure of Vat Brown BR and Vat Olive T are shown in Scheme S1, Supporting Information). The corresponding FESEM images (Figures S3 and S4, Supporting Information) reveal their morphologies are similar to those of VG 8/G composites. Specifically, the vat dyes are confined in the graphene layers when the weight ratio of vat dye to GO is 0.25 and 0.5, however, bulk particles are observed when the value is increased to 1. Thanks to the smart design and unique architectures, both composites manifest distinguished electrochemical performances when used as the cathodes for LIBs (Figures S5 and S6, Supporting Information). For example, pure Vat Brown BR and Vat Olive T do not have any electrochemical activities for Li storage with extremely low capacities (<10 mAh g^{-1}). Whereas, the VB BR/G and VO T/G composites display unexpectedly high Li storage capacities and particularly impressive rate capabilities. Especially, the VB BR/G-0.5 electrode delivers a high capacity of ≈270 mAh g^{-1} at a current density of 100 mA g^{-1} with no capacity fading after 200 continuous charge/discharge cycles, and meanwhile, a capacity of ≈41 mAh g^{-1} is still retained at a high current density of 3200 mA g^{-1}. In addition, the VO T/G-0.5 electrode also shows a high capacity of ≈240 mAh g^{-1} at 100 mA g^{-1} and good capacity retention at high charge rate (≈48 mAh g^{-1} at 3200 mA g^{-1}). These fascinating results highlight the applicability of our approach for other aromatic vat dyes toward low-cost and large-scale fabrication of high performance organic-based cathodes.

3. Conclusion

In summary, we have successfully developed a simple, universal, and scalable strategy to prepare the vat dye/graphene composite cathodes for LIBs. The hybridization process involves the disassembly of commercialized vat dye crystals along with their reassembly onto the graphene sheets by π–π supramolecular interactions. With this design, the accessibility of electrochemically active vat dye molecules to Li^+ ions could be significantly enhanced, and meanwhile their dissolution into the electrolyte could be effectively restrained. Furthermore, the unique structure is also beneficial for efficient electron transfer and shortens the Li^+ ions diffusion length. As a proof-of-concept demonstration, several types of vat dye/graphene composites, namely, VG 8/G, VB BR/G, and VO T/G, have been applied as cathodes for LIBs, which all exhibit excellent electrochemical performance with high Li storage capacity, good capacity retention, and advanced rate capability. Among them, VG 8/G-0.5 shows the best performance with a capacity of ≈272 mAh g^{-1} without any decay upon 200 consecutive cycles (at a current density of 100 mA g^{-1}) and superior rate performance (≈74 mAh g^{-1} at 3200 mA g^{-1}). It is believed that this work provides a facile and effective approach for engineering the organic cathodes toward high Li storage, and more meaningfully opens up new horizons in developing a versatile and cost-effective platform for large-scalable fabrication of advanced organic-based electrode materials for practical use.

4. Experimental Section

Preparation of GO Aqueous Solution: Graphite oxide was prepared by the well established oxidation route of graphite (China Jixi Jinyu Graphite Co., Ltd),[45] and then solution exfoliated into GO to form a homogeneous suspension.

Preparation of VG 8/G Composites: In a typical procedure, a precalculated amount (90, 180, and 360 mg) of Vat Green 8 (Xuzhou Kedah Fine Chemical Co., Ltd) was dispersed in 180 mL GO aqueous solution (2 mg mL^{-1}) under sustained sonication for 30 min. Then the resulting mixture was sealed in a 200 mL teflon autoclave and heated at

180 °C for 24 h. After the autoclave was naturally cooled down to room temperature, the formed hydrogel was taken out gently and rinsed with deionized water for several times to remove any impurities. Finally, the sample was freeze-dried in a freeze drying machine.

Preparation of Other Vat Dye/Graphene Composites: VB BR/G and VO T/G composites were prepared under the same experimental parameters, except the change of Vat Green 8 to Vat Brown BR or Vat Olive T.

Characterization: Powder XRD analysis was collected by using a Bruker D8 Advance X-Ray diffractometer. XPS measurements were conducted on an ESCALAB MK II instrument. Raman spectra were obtained on a WITec CRM200 Raman system using a 532 nm laser. FESEM images were recorded by a JEOL JSM-6700F scanning electron microscope. Nitrogen adsorption-desorption isotherms were performed on a Micromeritics Tristar II. TEM images were measured on a JEOL JEM-2010 transmission electron microscope. TGA was characterized under N_2 atmosphere using a Shimadzu DTG-60 H instrument. Elemental analysis was tested using a FLASH 2000 elemental analyzer.

Electrochemical Characterizations: Coin-type cells (CR2032) were assembled by sandwiching a porous polypropylene separator between a working electrode and a Li metal foil in a high-purity argon-filled glove box. 1 M $LiPF_6$ in a 1:1:1 (v/v) mixture of ethylene carbonate, ethyl methyl carbonate, and dimethyl carbonate was used as the electrolyte. The working electrodes were prepared by the conventional slurry-coating technique. Typically, the active material, acetylene black and poly (vinylidene fluoride) (PVDF) with a weight ratio of 7:2:1 were dissolved in N-methyl-2-pyrrolidinone to form a slurry, which was then spread on a aluminum foil and finally dried at 100 °C for 12 h in vacuum. Galvanostatic tests were conducted on a NEWARE battery test instrument in a voltage window of 1.20–4.20 V (vs Li/Li^+). Unless otherwise specified, all the specific capacities reported in this work are calculated based on the total mass of the electrode materials (excluding acetylene black and PVDF). The cells were pre-cycled at 10 mA g^{-1} for 10 cycles for activation before loaded to the test instrument. CV and EIS measurements were carried out on a CHI 760D electrochemical workstation.

Supporting Information

Supporting Information is available from the Wiley Online Library or from the author.

Acknowledgements

This work is supported by the A*STAR SERC PSF Grant 1321202101. W.H. thanks the support by the National Basic Research Program of China – Fundamental Studies of Perovskite Solar Cells (2015CB932200), Natural Science Foundation of Jiangsu Province (BM2012010), Priority Academic Program Development of Jiangsu Higher Education Institutions (YX03001), Ministry of Education of China (IRT1148), Synergetic Innovation Center for Organic Electronics and Information Displays, and the National Natural Science Foundation of China (61136003, 51173081). W.Z., Z.S., and J.Z. thank the support from National Natural Science Foundation of China (21663029, 21502091, and 51502060), Natural Science Foundation of Jiangsu Province (BK20130912 and 14KJB430017).

Received: July 17, 2016
Revised: August 17, 2016
Published online:

[1] Z. Yang, J. Zhang, M. C. W. Kintner-Meyer, X. Lu, D. Choi, J. P. Lemmon, J. Liu, *Chem. Rev.* **2011**, *111*, 3577.
[2] C. Liu, F. Li, L. P. Ma, H. M. Cheng, *Adv. Mater.* **2010**, *22*, E28.
[3] M. S. Whittingham, *MRS Bull.* **2008**, *33*, 411.
[4] W. Liu, P. Oh, X. Liu, M. J. Lee, W. Cho, S. Chae, Y. Kim, J. Cho, *Angew. Chem. Int. Ed.* **2015**, *54*, 4440.
[5] M. S. Islam, C. A. J. Fisher, *Chem. Soc. Rev.* **2014**, *43*, 185.
[6] N. Nitta, F. Wu, J. T. Lee, G. Yushin, *Mater. Today* **2015**, *18*, 252.
[7] Y. Liang, Z. Tao, J. Chen, *Adv. Energy Mater.* **2012**, *2*, 742.
[8] Z. Song, H. Zhou, *Energy Environ. Sci.* **2013**, *6*, 2280.
[9] J. Xie, Q. Zhang, *J. Mater. Chem. A* **2016**, *4*, 7091.
[10] H. Chen, M. Armand, M. Courty, M. Jiang, C. P. Grey, F. Dolhem, J. M. Tarascon, P. Poizot, *J. Am. Chem. Soc.* **2009**, *131*, 8984.
[11] H. Chen, M. Armand, G. Demailly, F. Dolhem, P. Poizot, J. M. Tarascon, *ChemSusChem* **2009**, *2*, 198.
[12] Y. Liang, P. Zhang, J. Chen, *Chem. Sci.* **2013**, *4*, 1330.
[13] B. Haupler, A. Wild, U. S. Schubert, *Adv. Energy Mater.* **2015**, *5*, 1402034.
[14] D. L. Williams, J. J. Byrne, J. S. Driscoll, *J. Electrochem. Soc.* **1969**, *116*, 2.
[15] Y. Morita, S. Nishida, T. Murata, M. Moriguchi, A. Ueda, M. Satoh, K. Arifuku, K. Sato, T. Takui, *Nat. Mater.* **2011**, *10*, 947.
[16] Y. Liang, P. Zhang, S. Yang, Z. Tao, J. Chen, *Adv. Energy Mater.* **2013**, *3*, 600.
[17] Z. Song, Y. Qian, X. Liu, T. Zhang, Y. Zhu, H. Yu, M. Otani, H. Zhou, *Energy Environ. Sci.* **2014**, *7*, 4077.
[18] W. Ai, Z. Du, Z. Fan, J. Jiang, Y. Wang, H. Zhang, L. Xie, W. Huang, T. Yu, *Carbon* **2014**, *76*, 148.
[19] B. Genorio, K. Pirnat, R. Cerc-Korosec, R. Dominko, M. Gaberscek, *Angew. Chem. Int. Ed.* **2010**, *49*, 7222.
[20] A. Jaffe, A. Saldivar Valdes, H. I. Karunadasa, *Chem. Mater.* **2015**, *27*, 3568.
[21] Z. Song, Y. Qian, M. L. Gordin, D. Tang, T. Xu, M. Otani, H. Zhan, H. Zhou, D. Wang, *Angew. Chem. Int. Ed.* **2015**, *54*, 13947.
[22] T. Nokami, T. Matsuo, Y. Inatomi, N. Hojo, T. Tsukagoshi, H. Yoshizawa, A. Shimizu, H. Kuramoto, K. Komae, H. Tsuyama, J. i. Yoshida, *J. Am. Chem. Soc.* **2012**, *134*, 19694.
[23] X. Han, C. Chang, L. Yuan, T. Sun, J. Sun, *Adv. Mater.* **2007**, *19*, 1616.
[24] Z. Zhu, M. Hong, D. Guo, J. Shi, Z. Tao, J. Chen, *J. Am. Chem. Soc.* **2014**, *136*, 16461.
[25] W. Huang, Z. Zhu, L. Wang, S. Wang, H. Li, Z. Tao, J. Shi, L. Guan, J. Chen, *Angew. Chem. Int. Ed.* **2013**, *52*, 9162.
[26] P. Zhou, J. Wang, F. Cheng, F. Li, J. Chen, *Chem. Commun.* **2016**, *52*, 6091.
[27] Z. Zhu, J. Chen, *J. Electrochem. Soc.* **2015**, *162*, A2393.
[28] M. Lee, J. Hong, H. Kim, H. D. Lim, S. B. Cho, K. Kang, C. B. Park, *Adv. Mater.* **2014**, *26*, 2558.
[29] S. Wang, L. Wang, K. Zhang, Z. Zhu, Z. Tao, J. Chen, *Nano Lett.* **2013**, *13*, 4404.
[30] K. Zhang, C. Guo, Q. Zhao, Z. Niu, J. Chen, *Adv. Sci.* **2015**, *2*, 1500018.
[31] Z. Song, T. Xu, M. L. Gordin, Y. B. Jiang, I. T. Bae, Q. Xiao, H. Zhan, J. Liu, D. Wang, *Nano Lett.* **2012**, *12*, 2205.
[32] H. Wang, P. Hu, J. Yang, G. Gong, L. Guo, X. Chen, *Adv. Mater.* **2015**, *27*, 2348.
[33] H. Zhang, Q. Deng, A. Zhou, X. Liu, J. Li, *J. Mater. Chem. A* **2014**, *2*, 5696.
[34] H. Mustroph, *Dyes, General Survey, in Ullmann's Encyclopedia of Industrial Chemistry*, Wiley-VCH Verlag GmbH & Co. KGaA, Weinheim **2014**, pp. 1–38.
[35] W. Ai, J. Jiang, J. Zhu, Z. Fan, Y. Wang, H. Zhang, W. Huang, T. Yu, *Adv. Energy Mater.* **2015**, *5*, 1500559.
[36] W. Ai, Z. Z. Du, J. Q. Liu, F. Zhao, M. D. Yi, L. H. Xie, N. E. Shi, Y. W. Ma, Y. Qian, Q. L. Fan, T. Yu, W. Huang, *RSC Adv.* **2012**, *2*, 12204.
[37] A. M. Rao, P. C. Eklund, S. Bandow, A. Thess, R. E. Smalley, *Nature* **1997**, *388*, 257.

[38] Z. Liu, K. Parvez, R. Li, R. Dong, X. Feng, K. Mullen, *Adv. Mater.* **2015**, *27*, 669.
[39] C. Luo, R. Huang, R. Kevorkyants, M. Pavanello, H. He, C. Wang, *Nano Lett.* **2014**, *14*, 1596.
[40] R. Zeng, L. Xing, Y. Qiu, Y. Wang, W. Huang, W. Li, S. Yang, *Electrochim. Acta* **2014**, *146*, 447.
[41] D. W. Wang, C. Sun, G. Zhou, F. Li, L. Wen, B. C. Donose, G. Q. Lu, H. M. Cheng, I. R. Gentle, *J. Mater. Chem. A* **2013**, *1*, 3607.
[42] W. Ai, Z. Luo, J. Jiang, J. Zhu, Z. Du, Z. Fan, L. Xie, H. Zhang, W. Huang, T. Yu, *Adv. Mater.* **2014**, *26*, 6186.
[43] W. Ai, J. Zhu, J. Jiang, D. Chao, Y. Wang, C. F. Ng, X. Wang, C. Wu, C. Li, Z. Shen, W. Huang, T. Yu, *2D Mater.* **2015**, *2*, 014005.
[44] S. S. Zhang, K. Xu, T. R. Jow, *Electrochim. Acta* **2004**, *49*, 1057.
[45] Z. Du, W. Ai, L. Xie, W. Huang, *J. Mater. Chem. A* **2014**, *2*, 9164.